



# Time-resolved photoacoustics of channelrhodopsins: early energetics and light-driven volume changes

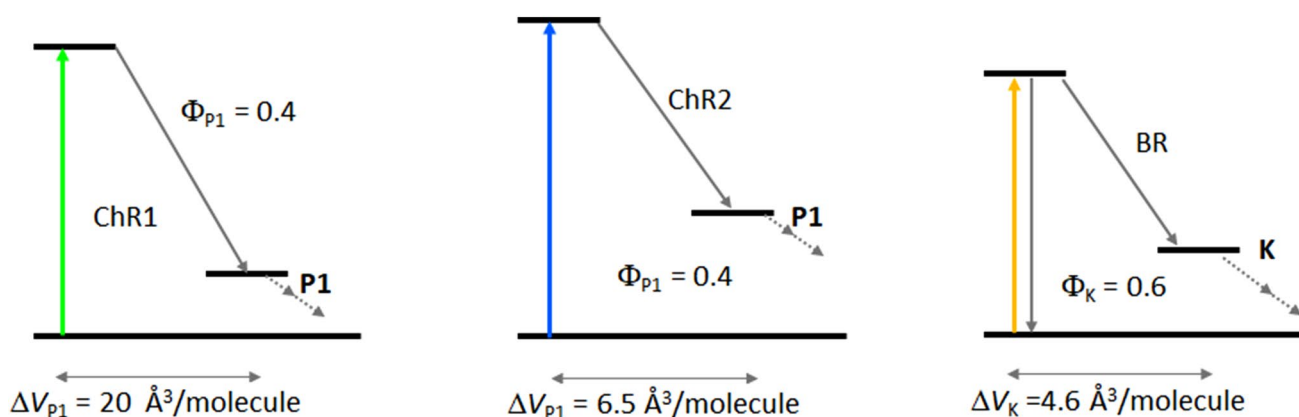
Maria Walter<sup>1</sup> · Luiz Schubert<sup>1</sup> · Joachim Heberle<sup>1</sup> · Ramona Schlesinger<sup>1</sup> · Aba Losi<sup>2</sup>

Received: 16 September 2022 / Accepted: 14 October 2022 / Published online: 23 October 2022  
© The Author(s) 2022

## Abstract

In biological photoreceptors, the energy stored in early transient species is a key feature to drive the photocycle or a chain of reactions. Time-resolved photoacoustics (PA) can explore the energy landscape of transient species formed within few ns after photoexcitation, as well as volumetric changes ( $\Delta V$ ) of these intermediates with respect to the parental state. In this work, PA identified these important parameters for several channelrhodopsins, namely *CaChR1* from *Chlamydomonas augustae* and *CrChR2* from *Chlamydomonas reinhardtii* and various variants. PA has access to the sub-ns formation of the early photoproduct P1 and to its relaxation, provided that this latter process occurs within a few  $\mu$ s. We found that  $\Delta V_{P1}$  for *CaChR1* is ca. 12 mL/mol, while it is much smaller for *CrChR2* (4.7 mL/mol) and for *H. salinarum* bacteriorhodopsin (*HsBR*,  $\Delta V_K = 2.8$  mL/mol). PA experiments on variants strongly indicate that part of this large  $\Delta V_{P1}$  value for *CaChR1* is caused by the protonation dynamics of the Schiff base counterion complex involving E169 and D299. PA data further show that the energy level of P1 is higher in *CrChR2* (ca. 96 kJ/mol) than in *CaChR1* (ca. 46 kJ/mol), comparable to the energy level of the K state of *HsBR* (60 kJ/mol). Instrumental to gain these molecular values from the raw PA data was the estimation of the quantum yield ( $\Phi$ ) for P1 formation via transient spectroscopy; for both channelrhodopsins,  $\Phi_{P2}$  was evaluated as ca. 0.4.

## Graphical Abstract



This article is dedicated to Silvia Braslavsky, for her first 80 years.

✉ Aba Losi  
aba.losi@unipr.it

<sup>1</sup> Department of Physics, Freie Universität Berlin, Arnimallee 14, 14195 Berlin, Germany

<sup>2</sup> Department of Mathematical, Physical and Computer Sciences, University of Parma, Parco Area Delle Scienze 7/A, 43124 Parma, Italy

## 1 Introduction

Photothermal methods such as time-resolved photoacoustics (PA) and thermal lensing give the unique opportunity to experimentally explore the thermodynamic landscape of light-triggered reactions by monitoring non-radiative decays accompanying excited state relaxation and formation of transient species [1, 2]. These features are especially relevant

for biological photoreceptors where absorption of photonic energy by chromophores triggers a photocycle or a chain of reactions, ultimately leading to the conversion of light energy into sensory photoresponses (e.g., vision, photomorphogenesis [3, 4]), chemical energy (e.g., photosynthesis [5]) or photoenzymatic activity (e.g., Photolyases [6]). The energetics of transient species following the decay of the chromophore excited state and the primary photochemistry is in general not easily dissected, but photothermal methods can determine the enthalpy changes ( $\Delta H$ ) with respect to the parental state by recovering non-radiative decays [7]. Another important outcome of time-resolved photothermal techniques is the determination of light-triggered volume changes ( $\Delta V$ ) of non-thermal origin that usually accompany the formation of transient species and may originate from diverse processes, such as rearrangements of weak interaction, ionization, space requiring photochemical reactions, protein conformational changes and light-triggered association/dissociation [1, 2, 7, 8]. With the support of steady-state and transient UV/Vis spectroscopy, it is possible to assign the signals acquired with photothermal methods and their dynamic evolution to specific steps of the light-triggered molecular events. This combined approach offers the possibility to recover relevant parameters, such as the energy content of reaction intermediates, their formation quantum yields ( $\Phi$ ), changes in photoreceptors shape or oligomerization and even optically silent transitions [1, 8, 9].

In this work, we used PA to investigate two members of the family of retinal binding photoreceptors, channelrhodopsin-1 from *Chlamydomonas augustae* (CaChR1) and channelrhodopsin-2 from *Chlamydomonas reinhardtii* (CrChR2). While in nature ChRs are involved in light sensing, they are utilized nowadays in optogenetic applications to stimulate neuronal cells by light [10]. Besides their role in the field of optogenetics, channelrhodopsins, as members of the family of microbial rhodopsins, are being intensively studied to derive biophysical concepts of membrane transport and sensing [10]. A central question is how the local perturbation of the retinal chromophore leads to structural changes within the apoprotein and subsequently to the respective physiological function. In microbial rhodopsins, light absorption leads in most cases to an all-*trans* to 13-*cis* isomerization of the retinal chromophore [11]. The photoreaction of retinal is highly selective and efficient in the binding pocket of the protein, ( $\Phi$  ca 0.6 for *Halobacterium salinarum* bacteriorhodopsin, *HsBR*) and occurs typically on a sub-ps timescale [12, 13]. In *HsBR*, about 30% of the absorbed photon energy is stored in the early photointermediate, K [14]. This stored energy can be rationalized by two factors: distortion of the retinal cofactor or weakened H-bonds destabilize the intermediate [11]. The subsequent relaxation of this energy during the decay of the early intermediate is believed to trigger global and

functionally relevant changes in the protein [11, 15]. It was shown for the red-activatable channelrhodopsin ReaChR that, depending on the protonation state of the counterion, either of the above-mentioned mechanisms for energy storage is favored but also the kinetics of the energy relaxation are affected [16].

In CaChR1 and CrChR2, large protein conformational changes are associated already with the early photointermediates (P1), as inferred from Fourier-transform infrared (FT-IR) experiments [17, 18]. This is in contrast to *HsBR*, where the major protein conformational changes are associated with the late N intermediate, that bears a reprotonated Schiff base but still a 13-*cis* retinal chromophore [19]; this fact is suggestive of two fundamentally different mechanisms of chromophore–protein interaction. Here, we report and compare PA-determined volumetric changes of channelrhodopsins and *HsBR* associated with the formation of the early photointermediates, as well as their energy levels. Remarkable differences in the prompt response after photoexcitation indicate that the downstream mechanism after photon absorption is different between the channelrhodopsins and the prototypical proton pump *HsBR*. In particular, ultrafast protonation dynamics of CaChR1 within the chromophore cavity [20, 21], involving Asp299 and Glu169, could be correlated with its much larger volume on the sub-ns timescale with respect to CrChR2, complementing the cited vibrational studies. Investigation of variants at D299 and E169 positions further confirmed these results. We also included PA measurements on CrChR2 mutated at Arg120: this residue belongs to the extracellular gate, thus strictly related to cation transport [22, 23]. Our data highlight that the R120H change does not affect the earliest energetics and volume changes, in line with the relevance of Arg120 for the later stages of the photocycle.

## 2 Materials and methods

### 2.1 Samples preparations and handling

Channelrhodopsins and their variants were prepared as described previously [24]. CaChR1 samples were stored in 20 mM HEPES, 100 mM NaCl, pH7.4, 0.03% DDM (*n*-Dodecyl- $\beta$ -D-maltopyranoside); CrChR2 samples were stored in the same buffer, but with 0.2% DM (*n*-Decyl- $\beta$ -D-maltopyranoside). *HsBR* in purple membrane patches in aqueous solutions (pH 6 and 100 mM NaCl) was kindly provided by Wolfgang Gärtner (University of Leipzig) and used as received, evaluating the scattering contribution by fitting the red flank of the absorption spectrum with a  $\lambda^{-4}$  function [25].

## 2.2 UV/Vis optical spectroscopy

Steady-state absorption and fluorescence spectroscopy measurements were carried out at  $20 \pm 1$  °C, respectively, with a Jasco 7850 UV/Vis spectrophotometer (Jasco Europe, Cremella, LC, Italy) and a PerkinElmer LS50 luminescence spectrometer (PerkinElmer, Waltham, MA, USA). For flash-photolysis experiments in the  $\mu\text{s}$ -to- $\text{ms}$  time range, samples were excited by a laser pulse (duration about 10 ns, energy kept around 1 mJ per pulse), obtained from an OPO (GWU Lasertechnik, Erfstadt, Germany), pumped by the third harmonic (355 nm) of a Q-switched Nd:YAG laser (InnoLas, Krailling, Germany) as described previously [26]. Kinetic traces were monitored using a further optical line: two monochromators (master and slave) selected the probe wavelength from a continuous-wave 75 W Xenon lamp (AMKO, Utting, Germany). The quantum yield ( $\Phi_{\text{M,X}}$ ) for the formation of the conducting intermediate P2 of the individual channelrhodopsin (corresponding to M for *HsBR*, bearing a deprotonated Schiff base) was evaluated from the maximum bleaching of the parent state at ca. 0.5 ms, using the comparative method that exploits a standard compound as an actinometer [27] (Eq. 1):

$$\Phi_{\text{P2,X}} = \Phi_{\text{ST}} \frac{\Delta A_{\text{X}}}{\Delta A_{\text{ST}}} \frac{\varepsilon_{\text{ST}}}{\varepsilon_{\text{X}}}, \quad (1)$$

where X and ST denote the sample to be measured and the standard compound, respectively.  $\Delta A$  and  $\varepsilon$  are the variation of absorbance and the absorption coefficients of the parent states at the probe wavelength; Eq. 1 implies that the two compounds have the same absorbance at the pump wavelength, i.e., the same amount of photons is absorbed, as well as the employment of the same pulse energy for excitation. In this work, we used *HsBR* as a standard compound as detailed in the text.

Absorption coefficients were determined as previously described [28]. Briefly, samples were illuminated with a portable LED torch, emitting cold white light with 180 lm, in the presence of 10 mM hydroxylamine until full conversion of retinal to retinal oxime was achieved. Subsequently, the solution was brought to pH 3. For the calculation of the absorption coefficients, the differential absorption coefficient for retinal oxime has been used ( $33,600 \text{ M}^{-1} \text{ cm}^{-1}$  at 360 nm) [29].

## 2.3 Pulsed photoacoustics

For time-resolved photoacoustic (PA) measurements excitation was achieved with the same ns laser as described above and as previously employed [26]. The samples (ca. 2.8 mL) were temperature controlled to  $\pm 0.02$  °C in the

cuvette holder FLASH 100 (Quantum Northwest, Spokane, WA, USA). PA signals detected by a V103-RM ultrasonic transducer were fed into a 5662 preamplifier (Panametrics Inc., Waltham, MA, USA). The laser beam was shaped by a  $1 \times 12$  mm slit. The pulse energy was measured with a pyroelectric energy meter (RJP735 head connected to a meter RJ7620 from Laser Precision Corp). The experiments were performed in the linear regime of amplitude versus laser fluence. The dye new coccine (FLUKA, Neu-Ulm, Germany) was used as a calorimetric reference [30]. PA signals were deconvoluted using the software Sound Analysis 3000 (Quantum Northwest Inc., Spokane, WA) assuming that the time evolution of the pressure is composed of a sum of exponential functions. This analysis yields the fractional amplitudes ( $\varphi_i$ ) and the lifetimes ( $\tau_i$ ) of the transients; the time window of PA is between 20 ns and 10  $\mu\text{s}$ , while the time resolution with the described slit is ca. 60 ns, as previously reported [26]. At a given temperature and for each resolved  $i$ -th step, the fractional amplitude (with respect to the reference compound)  $\varphi_i$  is the sum of the fraction of absorbed energy released as heat ( $\alpha_i$ ) and the structural (non-thermal) volume change ( $\Delta V_i$ ) per absorbed Einstein (mole of photons) according to Eq. 2 [31]:

$$\phi_i = \alpha_i + \frac{\Delta V_i c_p \rho}{E_\lambda \beta}, \quad (2)$$

where  $E_\lambda$  is the molar excitation energy,  $\beta = (1/V)(\partial V/\partial T)_p$  is the volume expansion coefficient,  $c_p$  is the heat capacity at constant pressure, and  $\rho$  is the mass density of the solvent. At each temperature, four deconvolution results were accumulated. The “two temperature” (TT) method was used to separate  $\alpha_i$  from  $\Delta V_i$  [1, 31]. The sample waveform was acquired at a temperature for which the thermal contribution to solvent expansion is zero,  $T_{\beta=0} = 1$  °C, and at the second, higher temperature,  $T_{\beta>0} = 10$  °C. The thermoelastic parameters of the solvent were determined by comparison with those of distilled water. At  $T_{\beta=0}$ , the sample signal is only due to  $\Delta V_i$ ; while at 10 °C, both heat release and  $\Delta V_i$  contribute. The reference was recorded at  $T_{\beta>0}$ . In some instances, we also applied the several temperature (ST) method, for which  $\alpha_i$  and  $\Delta V_i$  are determined from the linear plots of  $\varphi_i$  vs.  $c_p \rho / \beta$  [7].

In the case of channelrhodopsins, as for other retinal-based photoreceptors, the prompt PA signal ( $\tau_1 < 20$  ns) corresponds to the unresolved formation of the thermally relaxed K-like intermediate (called P1 in channelrhodopsins [32, 33]) after chromophore photoisomerisation; the subsequent relaxation of P1 can be detected and time-resolved in some variants, provided that the lifetime  $\tau_2$  for this process falls between ca. 60 ns and 5  $\mu\text{s}$ . Consequently, PA does not have in general access to the sub-ms formation of the P2 (M-like, deprotonated Schiff base) transient [7, 33, 34]. For

the prompt component, we develop Eq. 3 based on energy balance considerations:

$$\Phi_{P1} \frac{E_{P1}}{E_{\lambda}} = 1 - \alpha_i - \Phi_F \frac{E_F}{E_{\lambda}}, \quad (3)$$

where  $\Phi_F$  is the fluorescence quantum yield,  $E_F$  is the average energy for the fluorescence emission,  $E_{P1}$  is the energy content of the P1 intermediate and  $\Phi_{P1}$  is the quantum yield of its formation. The molecular volume changes that the proteins experience upon formation of P1 with respect to the parent state can be calculated from Eq. 4

$$\Delta V_{P1} = \frac{\Delta V_1}{\Phi_{P1}}. \quad (4)$$

Therefore, to determine the relevant molecular parameters  $E_{P1}$  and  $\Delta V_{P1}$ , the corresponding reaction quantum yields must be derived from other methodologies as detailed in the text.

### 3 Results and discussion

#### 3.1 Time-resolved photoacoustics

Figure 1 shows the PA signals, which could be successfully deconvoluted in some cases using a single exponential or a sum of two exponential terms yielding their decay lifetimes and fractional amplitudes. For each component, the  $\alpha_i$  and  $\Delta V_i$  “delta-V” parameters could then be readily determined using Eq. 2 and the methods described above.

The “prompt” PA signals ( $\tau_1 < 20$  ns) correspond to photoisomerisation of the all-*trans* retinal to 13-*cis* plus relaxations on the sub-ns timescale, eventually leading to the P1 intermediate (similar to the K state of *HsBR*) [7, 33–36]. PA provides values for the products  $\Phi_{P1}E_{P1}$  and  $\Phi_{P1}\Delta V_{P1}$  (Eq. 4), thereby furnishing a lower limit for  $\Phi_{P1}$  with the assumption that  $E_{P1} < E_{\lambda}$  (Table 1). Fluorescence was very low for all proteins analyzed and can be neglected in Eq. 3, giving the simplified Eq. 5:

$$\Phi_{P1}E_{P1} = (1 - \alpha_i) E_{\lambda}. \quad (5)$$

As in all retinal proteins reported in the literature, this step results in a positive structural volume change  $\Delta V_1$ , i.e., an expansion with respect to the unphotolysed state, at least partially related to retinal isomerization itself but certainly receiving contribution from other factors such as modifications of weak interactions or localized protein conformational changes [7]. For all ChR proteins investigated here, a large fraction of the absorbed energy is released as heat in this step ( $\alpha_i \geq 0.80$ ), again in agreement with other retinal proteins (see, for example, published data for *Natromonas pharaonis* halorhodopsin, *NpHR*, and *HsBR* in Table 1). The most striking result, though, is the much larger  $\Delta V_1$  measured for *CaChR1*-WT (4.90 ml/mol) compared to *CrChR2*-WT (1.55 ml/mol) (Table 1, Fig. 1). In the *CaChR1*-D299N variant, the value of  $\Delta V_1$  drops to 2.06 ml/mol, while the decrease is smaller in *CaChR1*-D299E. These data suggest that the larger  $\Delta V_1$  of *CaChR1*-WT reflects, at least partially, the peculiar ultrafast protonation dynamics within the chromophore cavity [20, 21]. In the parental state of

**Fig. 1** PA signals for four representative proteins at  $T_{\beta=0} = 1^\circ$  (green) and at  $T_{\beta>0} = 10^\circ\text{C}$  (blue), shown with waveforms of the reference compound new coccine at  $T_{\beta=0}$  (black) and at  $T_{\beta>0} = 10^\circ\text{C}$  (red)

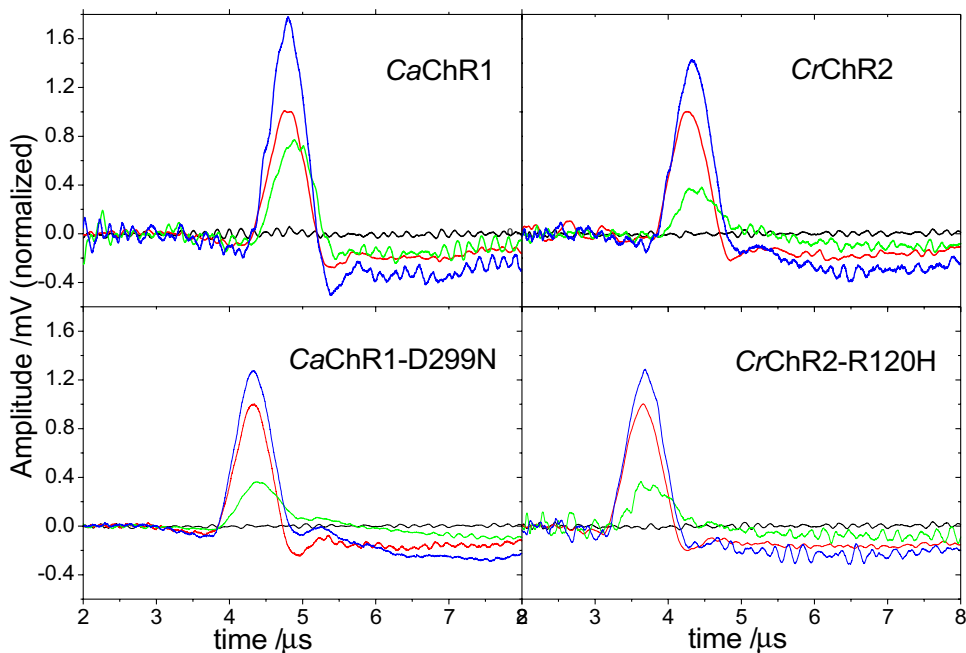


**Table 1** PA parameters measured for the “prompt” step ( $\tau < 20$  ns)

Protein	$\lambda_{ex}/nm$ ( $E_{\lambda}$ /kJ ml <sup>-1</sup> )	$\alpha_1$	$\Phi_{P1}$ $E_{P1}$ kJ/mol	$\Phi_{P1}$	$\Delta V_1$ ( $\Phi_{P1}\Delta V_{P1}$ ) ml/Einstein
<i>CaChR1</i> -WT	518 (230.9)	0.92 ± 0.05	18.5 ± 11.5	> 0.08 ± 0.05	4.90 ± 0.40
<i>CaChR1</i> -D299N	502 (238.3)	0.90 ± 0.04	23.8 ± 9.5	> 0.10 ± 0.04	2.06 ± 0.17
<i>CaChR1</i> -D299E	502 (238.3)	0.94 ± 0.06	14.7 ± 12.5	> 0.06 ± 0.05	2.80 ± 0.16
<i>CaChR1</i> -E169Q	508 (235.5)	0.92 ± 0.09	19.8 ± 15.5	> 0.08 ± 0.07	4.90 ± 0.30
<i>CrChR2</i> -WT	470 (254.5)	0.85 ± 0.03	38.2 ± 7.6	> 0.15 ± 0.03	1.55 ± 0.40
<i>CrChR2</i> -R120H	470 (254.5)	0.80 ± 0.02	50.9 ± 7.1	> 0.20 ± 0.02	1.74 ± 0.15
<i>NpHR</i> -Cl [56]	580 (206.2)	0.91 ± 0.04	16.6 ± 8.2	> 0.09 ± 0.04	10.0 ± 0.90
<sup>a</sup> <i>NpHR</i> -Cl	580 (206.2)	0.89 ± 0.04	22.7 ± 8.2	> 0.11 ± 0.04	9.2 ± 0.5
<sup>a</sup> <i>HsBR</i> [25]	568 (210.6)	0.83 ± 0.05	35.8 ± 10.5	> 0.17 ± 0.05	1.70 ± 0.20

<sup>a</sup>Membrane patches

*CaChR1*, the counterion complex of the protonated Schiff base comprises a neutral E169 (corresponding to the deprotonated *HsBR* D85 and *CrChR2* E123 [37]), a deprotonated D299 (*HsBR* D212 and D253 in *CrChR2*) and water molecules [20]. The retinal photoisomerisation occurs with a 110 fs time constant [21]. According to a recently proposed model, the ultrafast retinal isomerization promotes deprotonation of E169 concomitant to protonation of its backbone carbonyl group and formation of the first photoproduct within 300 fs [38]; alternatively, it was suggested that the E169 deprotonation/protonation pattern is triggered by a photoinduced ultrafast electron density translocation along the retinal chromophore polyene chain; this process is proposed to be independent of the photoisomerisation [20]. In any case, the proton of E169 is transferred to D299 at 30 ps [38]. This concurs with the finding that replacement of D299 by asparagine (D299N) short-circuits this proton dynamics; furthermore, E169 is deprotonated in the parental state of *CaChR1*-D299N [39]. The large  $\Delta V_1$  observed in *CaChR1*-WT, thus, most probably includes the ultrafast protonation of D299; in agreement with this hypothesis, the mutation E169Q does not exert any effect on  $\Delta V_1$  (Table 1).

Different to *CaChR1*, in *CrChR2*, both residues E123 and D253 become protonated concomitantly with Schiff

base deprotonation and formation of P2 on the hundreds of  $\mu$ s timescale [37, 40], i.e., outside the time window of PA. Besides *CrChR2*-WT, we have also investigated the variant R120H; R120 is located on helix C between the Schiff base counterions E123 and D253 and is part of the extracellular gate [22, 23]; the mutation R120H results in loss of *CrChR2* function as cation channel, but does not appreciably affect the spectroscopic features of the photocycle and the early dynamics [41]. Accordingly, we did not detect any appreciable differences in the PA data, with the only exception of the lifetime associated with the relaxation step of P1 ( $\tau_2$ , Table 2). We point out that only some of the proteins analyzed here have a relaxation of P1 short enough to fall within the time window of PA, including *CrChR2*-Wt and *CrChR2*-R120H (Table 2). The  $\tau_2 = 450$  ns for *CrChR2*-WT (at 10 °C, 254 ns at 20 °C) should correspond to the time constant of 400 ns reported for the optically transient transition between P1a and P1b detected using step-scan FT-IR spectroscopy [40], while we do not have comparable data for this transition from other spectroscopic methods for the R120H variant that appears slightly faster from our data. Small expansions have been reported for *NpHR* and *HsBR* on the hundreds of ns-to-short  $\mu$ s timescale, corresponding to K decaying into the L intermediate (Table 2).

**Table 2** PA parameters measured for a time-resolved step

Protein	$\alpha_2$	$\Phi_2\Delta V_2$ ml/mol	$\Phi_2 E_2$ kJ/mol	$\tau_2$ at 10 °C/ns	Proposed process
<i>CaChR1</i> -D299N	0.08 ± 0.07	5.60 ± 0.60	3.0 ± 22	1400 ± 60	Initial formation of P2 [42]
<i>CrChR2</i> -WT	0.09 ± 0.03	2.70 ± 0.35	13.8 ± 4.8	450 ± 47	P1a-to-P1b decay [40]
<i>CrChR2</i> -R120H	0.10 ± 0.02	2.10 ± 0.30	26.7 ± 5.6	270 ± 20	P1a-to-P1b decay [40]
<i>NpHR</i> -Cl [56]	0.02 ± 0.02	0.54 ± 0.04	27 ± 11	370 ± 40	
<sup>a</sup> <i>NpHR</i> -Cl [56]	0.02 ± 0.02	0.53 ± 0.15	36 ± 11	740 ± 60	
<sup>a</sup> <i>HsBR</i> [25]	0.06 ± 0.02	0.80 ± 0.06	23.5 ± 12.0	<sup>b</sup> 1000 ± 64	K-to-L

<sup>a</sup>Membrane patches

<sup>b</sup>20 °C

For *CaChR1*-Wt, the decay of P1 falls outside the PA time window; while for *CaChR1*-D299N, the formation of P2 (M-like, with deprotonated Schiff base) is faster, without any loss of its quantum yield with respect to the wt protein [42]: in *CaChR1*-D299N the rise of P2 is a three-exponential process characterized by lifetimes 1.5  $\mu\text{s}$ , 75  $\mu\text{s}$ , and 3.3 ms, the fastest of which should correspond to the value of 1.4  $\mu\text{s}$  recovered with PA (Table 2). A second and larger expansion  $\Delta V_2$  accompanies this step (Table 2). The corresponding lifetimes in *CaChR1*-WT and *CaChR1*-E169Q are 20  $\mu\text{s}$  and 65  $\mu\text{s}$ , respectively [42].

The linear Arrhenius plots (Fig. 2) confirm that  $\tau_2$  characterizes a *bona fide* relaxation of P1 and underscore the different nature of this step between *CrChR2* variants and *CaChR1*-D299: in the latter protein, the activation energy  $E_a$  is smaller than that for the other two proteins, but the larger  $\tau_2$  is justified by a much smaller pre-exponential factor, suggesting that the activation entropy is less favorable.

### 3.2 Quantum yield determination of channelrhodopsins

Given that PA can directly record solely the values of  $\Delta V_s$  per *mole* of absorbed photons, the large difference in  $\Phi_{P1}\Delta V_{P1}$  between *CaChR1* and *CrChR2* must be validated upon evaluation of the formation quantum yield for P1 to obtain the molecular values for the structural volume changes ( $\Delta V_{P1}$ ). The large spectral overlap between P1 and the parental state in channelrhodopsins [42–44] impairs the direct determination of  $\Phi_{P1}$  by means of transient UV–Vis spectroscopy. On the contrary, the Schiff

base in the P2 (M-like) intermediate is deprotonated and the large blue shift of the absorption spectrum ensures minimal overlap with the parental state [34, 42–44]. Thus, to apply Eq. 1 for the evaluation of  $\Phi_{P2}$ , the absorption coefficients ( $\epsilon$ ) of the parental state must be determined under our working conditions according to the procedure described in the Materials and Methods section. After formation of retinal oxime, it is evident that the maximum value of  $\epsilon$  is very similar of intact, solubilized *CaChR1* and *CrChR2* (Fig. 3a), although somehow contrasting values are reported in the literature, i.e., 36,000  $\text{M}^{-1}\text{cm}^{-1}$  for *CaChR1* at 518 nm [45] and 45,500 for *Volvox carteri* VChR2  $\text{M}^{-1}\text{cm}^{-1}$  at 470 nm [46]. The discrepancy may be due to the different employed values of  $\epsilon$  for retinal oxime at 360 nm (33,600  $\text{M}^{-1}\text{cm}^{-1}$  [45] and 54,000  $\text{M}^{-1}\text{cm}^{-1}$  [47], respectively). Bearing in mind that 33,600  $\text{M}^{-1}\text{cm}^{-1}$  was defined as differential coefficient [45], thus giving in the present case  $\epsilon_{519} = 43,000\text{ M}^{-1}\text{cm}^{-1}$  for *CaChR1* and  $\epsilon_{474} = 45,000\text{ M}^{-1}\text{cm}^{-1}$  for *CrChR2* (Fig. 3b). These values can be compared with the  $\epsilon_{568} = 62,700\text{ M}^{-1}\text{cm}^{-1}$  for *HsBR* in purple membranes, based on binding of all-*trans* retinal and its value of  $\epsilon_{382} = 42,800\text{ M}^{-1}\text{cm}^{-1}$  [48]. Consistent with the obtained slightly lower values of absorption coefficients for channelrhodopsins, *HsBR* exhibits a higher absorbance before the transformation of its chromophore to retinal oxime [49, 50].

Comparing the maximum bleaching of *HsBR* and *CrChR2* at 5 ms (pump beam at 502 nm, probe beam at 568 and 474 nm, respectively), we obtained a value of  $\Phi_{P2,\text{CHR2}} = 0.40$  using  $\Phi_{M,\text{BR}} = 0.60$  in Eq. 1 [51]. This value now is applied for *CrChR2* to measure the corresponding quantum yield for *CaChR1* (pump beam at 488 nm, probe beam at 474 and 519 nm respectively), obtaining  $\Phi_{P2,\text{CHR1}} = 0.40$ . These results can be compared with the value of  $\Phi_{P1} = 0.3$  previously measured for the chimeric C1C2 protein [52]; in the C1C2 chimera, helices I–V derive from *CrChR1*, while helices VI–VII derive from *CrChR2* [53]. A similar  $\Phi_{L,\text{HR}} = 0.34$  has been reported for the photocycle of *HsHR* [54]. In slight contrast, a value of ca. 0.6 for photoisomerization in *CrChR2* was recently reported, as derived from theoretical calculations and simulations for photoisomerization [55]. Notably, this last value was determined from ultrafast dynamics of the chromophore, i.e., it is not affected by possible side reactions occurring on the tens of ns-to-ms timescale.

For the calculation of the molecular volume change associated with the formation of P1 and of the energy level of the same intermediate, we assume in the following that  $\Phi_{P1} = \Phi_{P2}$ , i.e., that the P1-to-P2 conversion is quantitative, as previously done for other retinal proteins [7, 25, 56].

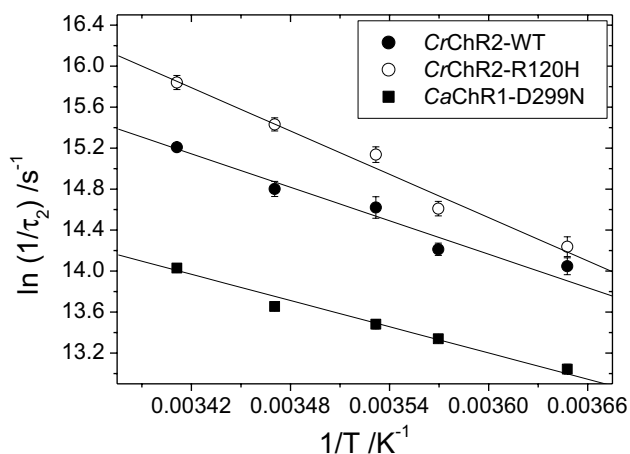


**Fig. 2** Arrhenius plots for the three proteins for which  $\tau_2$  was measurable with PA, between the temperature range from 1 to 20 °C. From the slopes of the linear plots ( $R \geq 0.99$ ), the following activation energies  $E_a$  and the pre-exponential factors  $A$  were determined: *CrChR2*-WT,  $E_a = 45\text{ kJ/mol}$  and  $A = 4.6 \times 10^{14}$ ; *CrChR2*-R120H,  $E_a = 58\text{ kJ/mol}$  and  $A = 2.1 \times 10^{17}$ ; *CaChR1*-D299N,  $E_a = 35\text{ kJ/mol}$  and  $A = 2.5 \times 10^{12}$ .

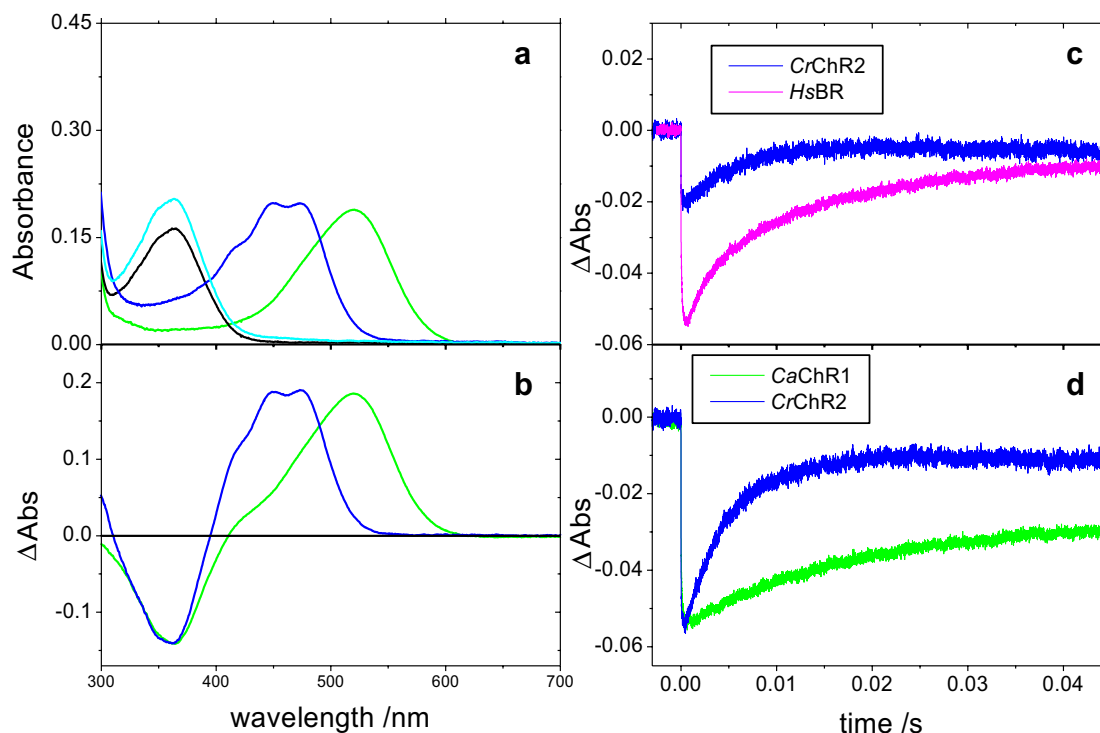


**Fig. 3** **a** Absorption spectra of *CaChR1* and *CrChR2* before (green and blue, respectively) and after (black and cyan) treatment with 10 mM hydroxylamine and cold white light to generate retinal oxime; **b** Differential spectra extracted from spectra in **a**, where negative  $\Delta\text{Abs}$  reflects retinal oxime formation; **c** transient absorbance changes for *HsBR* (magenta) and *CrChR2* (blue), with pump beam at 502 nm,

probe beam at 568 and 474 nm, respectively; **d** transient absorbance changes for *CrChR2* (blue) and *CaChR1* (green), with pump beam at 488 nm, probe beam at 474 nm and 519 nm, respectively; in both cases, absorbance at the pump wavelength and the laser energy were matched between the different samples

### 3.3 Energetics of the P1 intermediate in *CaChR1* and *CrChR2*

The primary photoproduct in microbial rhodopsins (K, the K-like or P1 states), which rises in the sub-ns timescale after all-*trans* to 13-*cis* photoisomerisation of the retinal chromophore, stores an amount of energy required to drive the rest of the photocycle [7]. PA intrinsically detects variation in enthalpy ( $\Delta H$ ), i.e., non-radiative decays, but assuming that entropic changes are negligible for the fast formation of P1  $E_{P1} \approx \Delta H_{P1}$ , we can calculate the energy level of this intermediate with respect to the unphotolysed state, according to eqs. 3 and 5. The results are visualized in Fig. 4 together with the molecular volume change of the non-thermal origin ( $\Delta V_{P1}$ ) accompanying this step.

By using Eq. 5 to extract the PA data reported in Table 1 and normalized by the measured  $\Phi_{P1}$ s, it can be calculated that the P1 intermediate in *CaChR1* stores about 20% of the excitation energy ( $E_{P1} = 46 \pm 29$  kJ/mol), while the corresponding value for *CrChR2* is 37% ( $E_{P1} = 95 \pm 19$  kJ/mol). Although it is tempting to speculate that the energy level of P1 is inversely correlated with  $\Delta V_{P1}$ , the results obtained for *CaChR1*-D299N show that this is not the case: the value

of  $E_{P1}$  for this variant can be evaluated as  $E_{P1} = 59 \pm 24$  kJ/mol from  $\alpha_1$  (Table 1) and the assumption that the quantum efficiency is the same as in the wt protein [42]. Thus, it follows that  $E_{P1}$  is essentially the same as for *CaChR1*; nevertheless,  $\Delta V_{P1} = 5.1 \pm 0.4$  mL/mol for this variant, which is much smaller than the value of  $\Delta V_{P1} = 12.2 \pm 1.0$  mL/mol of *CaChR1*.

For both *CaChR1* and *CrChR2*,  $\Delta V_{P1}$  is larger than the corresponding  $\Delta V_K = 2.8$  mL/mol for *HsBR* [25]. Using FT-IR spectroscopy, it was demonstrated that the formation of P1 in the two channelrhodopsins implies significant protein conformational changes, in contrast to *HsBR* [18], thereby suggesting such a contribution also to the PA-derived  $\Delta V_{P1}$ . In general, the sources for  $\Delta V$ s measured with PA are not easily assigned: they can comprise electrostriction around newly formed charges, changes in the geometry of the chromophore that result in rearrangements of weak interactions, and/or protein structural changes [1]. On the relatively fast time window of PA (up to a few  $\mu$ s), large protein conformational changes are in general not expected for photoreceptors but cannot be excluded here because of the supporting evidence from vibrational spectroscopy as mentioned above. According to recently published data,

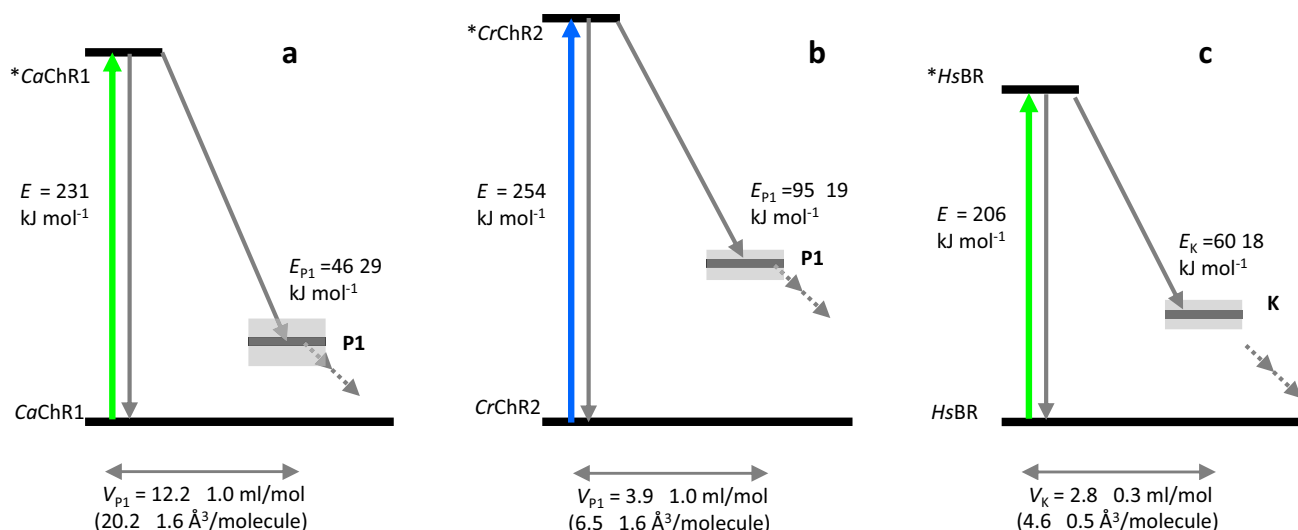


**Fig. 4** Energy diagram for the sub-ns formation of the P1 intermediate in **a** *CaChR1* and **b** *CrChR2*, as derived from PA measurements and evaluation of  $\Phi_{P1}$  (0.4, vide supra). Shaded boxes indicate the magnitude of the error related to the energy level of P1. Colored arrows stand for the excitation energy  $E_i$ ; dark gray arrows indicate the thermal decay processes detected with PA; dotted double arrows

stand for the completion of the photocycle. At the bottom, the PA-derived structural volume changes accompanying the formation of P1 are shown ( $\Delta V_{P1}$ ). For comparison, data for K formation in *HsBR* are also shown (c). To appreciate the magnitude of the  $\Delta V$ s consider that water occupies 18 ml/mol (29.9 Å<sup>3</sup>/molecule)

the protonation state of the main counterion (D85 in *HsBR*, E123 in *CrChR2*, and E169 in *CaChR1*) can determine the efficiency of energy transfer from the photoisomerized chromophore to the protein [16]: in particular, in the red-shifted channelrhodopsin variant ReaChR, when the main counterion is protonated, the hydrogen bonds (HB) network in the chromophore cavity is more rigid and the distorted isomerized chromophore conformation is stabilized, rendering the dynamics of energy transfer from chromophore to protein slower [16]. The PA-derived data (Fig. 3) seem to confirm this suggestion for the channelrhodopsins, given that E169 is protonated in the ground state of *CaChR1*, while E123 of *CrChR2* is deprotonated. Nevertheless, in *CaChR1*-D299, for which E169 is dissociated in the parental state [39], the energy level of P1 is not substantially different from *CaChR1* (vide supra) (Fig. 3). The presence of a more rigid hydrogen-bonded network, though, can at least partially account for the larger  $\Delta V_{P1}$  in *CaChR1*;  $\Delta V_{P1}$  for this protein is comparable to the  $\Delta V_K = 19.2$  mL/mol measured for *NpHR*, when loaded with Cl<sup>-</sup> [56].

## 4 Conclusions

The PA data reported here have evidenced that the structural volume changes ( $\Delta V_{P1}$ ) accompanying the formation of P1 in *CaChR1* is ca. 3.5-fold larger than the corresponding  $\Delta V_{P1}$  of *CrChR2*. The analysis of variants

demonstrates that this large difference is related to the ultrafast protonation dynamics of the counterion complex in *CaChR1*, in particular the large contribution may originate from the ultrafast protonation of the backbone carbonyl of E169 by D299. A further contribution to the measured  $\Delta V_{P1}$ s for channelrhodopsins could derive from protein conformational changes concomitant with the formation of P1, as previously evidenced by time-resolved vibrational spectroscopy, in sharp contrast to *HsBR* [18]. PA data, thus, confirm that structural changes occurring on the sub-nanosecond timescale set the stage for the further conformational modifications leading to opening of the channel. In *CaChR1*, P1 stores a considerably smaller amount of energy than P1 in *CrChR2*, but a link with the slower decay of this intermediate into P2 for the former could not be firmly established. In agreement with other microbial rhodopsins, a large fraction of the excitation energy is released as heat upon formation of K or P1, in contrast to bovine rhodopsin where the batho-intermediate stores > 90% of the excitation energy [7]. This finding suggests that the completion of the photocycle must be driven also by favorable entropic changes. Essential for the here drawn conclusions is the determination of the quantum yield of the photocycle (formation of P2) that were demonstrated to be very similar for *CaChR1* and *CrChR2*, i.e., ca. 0.4.

**Acknowledgements** We thank Kirsten Hoffmann and Dorothea Heinrich for the skillful sample preparation. This work was supported by

the German Research Foundation through SFB1078 projects B3 (J.H.) and B4 (R.S.).

**Funding** Open access funding provided by Università degli Studi di Parma within the CRUI-CARE Agreement.

## Declarations

**Conflict of interest** The authors have no competing interests to declare that are relevant to the content of this article.

**Open Access** This article is licensed under a Creative Commons Attribution 4.0 International License, which permits use, sharing, adaptation, distribution and reproduction in any medium or format, as long as you give appropriate credit to the original author(s) and the source, provide a link to the Creative Commons licence, and indicate if changes were made. The images or other third party material in this article are included in the article's Creative Commons licence, unless indicated otherwise in a credit line to the material. If material is not included in the article's Creative Commons licence and your intended use is not permitted by statutory regulation or exceeds the permitted use, you will need to obtain permission directly from the copyright holder. To view a copy of this licence, visit <http://creativecommons.org/licenses/by/4.0/>.

## References

- Gensch, T., & Viappiani, C. (2003). Time-resolved photothermal methods: Accessing time-resolved thermodynamics of photoinduced processes in chemistry and biology. *Photochemical & Photobiological Sciences*, 2(7), 699–721.
- Proskurnin, M. A., Khabibullin, V. R., Usoltseva, L. O., Vyrko, E. A., Mikheev, I. V., & Volkov, D. S. (2022). Photothermal and optoacoustic spectroscopy: State of the art and prospects. *Physics-Uspekhi*, 65(3), 270–312.
- Kandori, H. (2020). Biophysics of rhodopsins and optogenetics. *Biophysical Reviews*, 12(2), 355–361.
- Kottke, T., Xie, A., Larsen, D. S., & Hoff, W. D. (2018). Photoreceptors take charge: emerging principles for light sensing. *Annual Review of Biophysics*, 47, 291–313.
- Stürbet, A., Lázár, D., Guo, Y., & Govindjee, G. (2020). Photosynthesis: Basics, history and modelling. *Annals of Botany*, 126(4), 511–537.
- Björn, L. O. (2018). Photoenzymes and related topics: An update. *Photochemistry and Photobiology*, 94(3), 459–465.
- Losi, A., & Braslavsky, S. E. (2003). The time-resolved thermodynamics of the chromophore–protein interactions in biological photosensors as derived from photothermal measurements. *Physical Chemistry Chemical Physics*, 5(13), 2739–2750.
- Terazima, M. (2021). Time-resolved detection of association/dissociation reactions and conformation changes in photosensor proteins for application in optogenetics. *Biophysical Reviews*, 13(6), 1053–1059.
- Losi, A., Bonomi, H. R., Michael, N., Tang, K., & Zhao, K.-H. (2017). Time-resolved energetics of photoprocesses in prokaryotic phytochrome-related photoreceptors. *Photochemistry and Photobiology*, 93(3), 733–740.
- Govorunova, E. G., Sineshchekov, O. A., Li, H., & Spudich, J. L. (2017). Microbial rhodopsins: Diversity, mechanisms, and optogenetic applications. *Annual Review of Biochemistry*, 86, 845–872.
- Ernst, O. P., Lodowski, D. T., Elstner, M., Hegemann, P., Brown, L. S., & Kandori, H. (2014). Microbial and animal rhodopsins: Structures, functions, and molecular mechanisms. *Chemical Reviews*, 114(1), 126–163.
- Tittor, J., & Oesterhelt, D. (1990). The quantum yield of bacteriorhodopsin. *FEBS Letters*, 263(2), 269–273.
- Govindjee, R., Balashov, S. P., & Ebrey, T. G. (1990). Quantum efficiency of the photochemical cycle of bacteriorhodopsin. *Biophysical Journal*, 58(3), 597–608.
- Birge, R. R., & Cooper, T. M. (1983). Energy storage in the primary step of the photocycle of bacteriorhodopsin. *Biophysical Journal*, 42(1), 61–69.
- Lórenz-Fonfría, V. A., Bamann, C., Resler, T., Schlesinger, R., Bamberg, E., & Heberle, J. (2015). Temporal evolution of helix hydration in a light-gated ion channel correlates with ion conductance. *Proceedings of the National Academy of Sciences of the United States of America*, 112(43), E5796–E5804.
- Kaufmann, J. C. D., Krause, B. S., Adam, S., Ritter, E., Schapiro, I., Hegemann, P., et al. (2020). Modulation of light energy transfer from chromophore to protein in the channelrhodopsin ReaChR. *Biophysical Journal*, 119(3), 705–716.
- Radu, I., Bamann, C., Nack, M., Nagel, G., Bamberg, E., & Heberle, J. (2009). Conformational changes of channelrhodopsin-2. *Journal of the American Chemical Society*, 131(21), 7313–7319.
- Ogren, J. I., Yi, A., Mamaev, S., Li, H., Lugtenburg, J., DeGrip, W. J., et al. (2015). Comparison of the structural changes occurring during the primary phototransition of two different channelrhodopsins from *Chlamydomonas algae*. *Biochemistry*, 54(2), 377–388.
- Souvignier, G., & Gerwert, K. (1992). Proton uptake mechanism of bacteriorhodopsin as determined by time-resolved stroboscopic-FTIR-spectroscopy. *Biophysical Journal*, 63(5), 1393–1405.
- Heyne, K. (2022). Impact of ultrafast electric field changes on photoreceptor protein dynamics. *The Journal of Physical Chemistry B*, 126(3), 581–587.
- Stensitzki, T., Yang, Y., Muders, V., Schlesinger, R., Heberle, J., & Heyne, K. (2016). Femtosecond infrared spectroscopy of channelrhodopsin-1 chromophore isomerization. *Structural Dynamics*, 3(4), 043208.
- Yang, T., Zhang, W., Cheng, J., Nie, Y., Xin, Q., Yuan, S., et al. (2019). Formation mechanism of ion channel in channelrhodopsin-2: Molecular dynamics simulation and steering molecular dynamics simulations. *International Journal of Molecular Sciences*, 20(15), 3780.
- Plazzo, A. P., De Franceschi, N., Da Broi, F., Zonta, F., Sanasi, M. F., Filippini, F., et al. (2012). Bioinformatic and mutational analysis of channelrhodopsin-2 protein cation-conducting pathway. *Journal of Biological Chemistry*, 287(7), 4818–4825.
- Walter, M., & Schlesinger, R. (2021). Nanodisc reconstitution of channelrhodopsins heterologously expressed in *pichia pastoris* for biophysical investigations. *Methods in Molecular Biology*, 2191, 29–48.
- Losi, A., Michler, I., Gärtner, W., & Braslavsky, S. E. (2000). Time-resolved thermodynamic changes photoinduced in 5,12-trans-locked bacteriorhodopsin. Evidence that retinal isomerization is required for protein activation. *Photochemistry and Photobiology*, 72(5), 590.
- Ding, Y., Zhao, Z., Matysik, J., Gärtner, W., & Losi, A. (2021). Mapping the role of aromatic amino acids within a blue-light sensing LOV domain. *Physical Chemistry Chemical Physics*, 23(31), 16767–16775.
- Ni, W., Gurzadyan, G. G., Zhao, J., Che, Y., Li, X., & Sun, L. (2019). Singlet fission from upper excited electronic states of cofacial perylene dimer. *The Journal of Physical Chemistry Letters*, 10(10), 2428–2433.
- Iwamoto, M., Sudo, Y., Shimono, K., & Kamo, N. (2001). Selective reaction of hydroxylamine with chromophore during

- the photocycle of pharaonis phoborhodopsin. *Biochimica et Biophysica Acta (BBA) - Biomembranes*, 1514(1), 152–158.
29. Scharf, B., Hess, B., & Engelhard, M. (1992). Chromophore of sensory rhodopsin II from *Halobacterium halobium*. *Biochemistry*, 31(49), 12486–12492.
  30. Abbruzzetti, S., Viappiani, C., Murgida, D. H., Erra-Balsells, R., & Bilmes, G. M. (1999). Non-toxic, water-soluble photocalorimetric reference compounds for UV and visible excitation. *Chemical Physics Letters*, 304(3–4), 167–172.
  31. Braslavsky, S. E., & Heibel, G. E. (1992). Time-resolved photothermal and photoacoustic methods applied to photoinduced processes in solution. *Chemical Reviews*, 92(6), 1381–1410.
  32. Lórenz-Fonfría, V. A., Resler, T., Krause, N., Nack, M., Gossing, M., Fischer von Mollard, G., et al. (2013). Transient protonation changes in channelrhodopsin-2 and their relevance to channel gating. *Proceedings of the National Academy of Sciences of the United States of America*, 110(14), E1273–E1281.
  33. Stensitzki, T., Muders, V., Schlesinger, R., Heberle, J., & Heyne, K. (2015). The primary photoreaction of channelrhodopsin-1: Wavelength dependent photoreactions induced by ground-state heterogeneity. *Frontiers in Molecular Biosciences*, 2, 41.
  34. Oda, K., Nomura, T., Nakane, T., Yamashita, K., Inoue, K., Ito, S., et al. (2021). Time-resolved serial femtosecond crystallography reveals early structural changes in channelrhodopsin. *eLife*, 10, e62389.
  35. Neumann-Verhoeven, M. K., Neumann, K., Bamann, C., Radu, I., Heberle, J., Bamberg, E., et al. (2013). Ultrafast infrared spectroscopy on channelrhodopsin-2 reveals efficient energy transfer from the retinal chromophore to the protein. *Journal of the American Chemical Society*, 135(18), 6968–6976.
  36. Schnedermann, C., Muders, V., Ehrenberg, D., Schlesinger, R., Kukura, P., & Heberle, J. (2016). Vibronic dynamics of the ultrafast all-trans to 13-cis photoisomerization of retinal in channelrhodopsin-1. *Journal of the American Chemical Society*, 138(14), 4757–4762.
  37. Kottke, T., Lórenz-Fonfría, V. A., & Heberle, J. (2017). The grateful infrared: Sequential protein structural changes resolved by infrared difference spectroscopy. *The Journal of Physical Chemistry B*, 121(2), 335–350.
  38. Stensitzki, T., Adam, S., Schlesinger, R., Schapiro, I., & Heyne, K. (2020). Ultrafast backbone protonation in channelrhodopsin-1 captured by polarization resolved fs Vis-pump—IR-probe spectroscopy and computational methods. *Molecules*, 25(4), 848.
  39. Ogren, J. I., Yi, A., Mamaev, S., Li, H., Spudich, J. L., & Rothschild, K. J. (2015). Proton transfers in a channelrhodopsin-1 studied by fourier transform infrared (FTIR) difference spectroscopy and site-directed mutagenesis. *Journal of Biological Chemistry*, 290(20), 12719–12730.
  40. Lórenz-Fonfría, V. A., Schultz, B.-J., Resler, T., Schlesinger, R., Bamann, C., Bamberg, E., et al. (2015). Pre-gating conformational changes in the ChETA variant of channelrhodopsin-2 monitored by nanosecond IR spectroscopy. *Journal of the American Chemical Society*, 137(5), 1850–1861.
  41. Resler, T. (2016). *Time-resolved analysis of protonation dynamics in channelrhodopsin-2*. Freie Universität Berlin.
  42. Sineshchekov, O. A., Govorunova, E. G., Wang, J., Li, H., & Spudich, J. L. (2013). Intramolecular proton transfer in channelrhodopsins. *Biophysical Journal*, 104(4), 807–817.
  43. Bamann, C., Kirsch, T., Nagel, G., & Bamberg, E. (2008). Spectral characteristics of the photocycle of channelrhodopsin-2 and its implication for channel function. *Journal of Molecular Biology*, 375(3), 686–694.
  44. Verhoeven, M. K., Bamann, C., Blöcher, R., Förster, U., Bamberg, E., & Wachtveitl, J. (2010). The photocycle of channelrhodopsin-2: Ultrafast reaction dynamics and subsequent reaction steps. *ChemPhysChem*, 11(14), 3113–3122.
  45. Muders, V., Kerruth, S., Lórenz-Fonfría, V. A., Bamann, C., Heberle, J., & Schlesinger, R. (2014). Resonance Raman and FTIR spectroscopic characterization of the closed and open states of channelrhodopsin-1. *FEBS Letters*, 588(14), 2301–2306.
  46. Ernst, O. P., Murcia, P. A. S., Daldrop, P., Tsunoda, S. P., Kateriya, S., & Hegemann, P. (2008). Photoactivation of channelrhodopsin. *Journal of Biological Chemistry*, 283(3), 1637–1643.
  47. Groenendijk, G. W. T., de Grip, W. J., & Daemen, F. J. M. (1979). Identification and characterization of syn- and anti-isomers of retinaloximes. *Analytical Biochemistry*, 99(2), 304–310.
  48. Rehorek, M., & Heyn, M. P. (1979). Binding of all-trans-retinal to the purple membrane. Evidence for cooperativity and determination of the extinction coefficient. *Biochemistry*, 18(22), 4977–4983.
  49. Subramaniam, S., Marti, T., Rosselet, S. J., Rothschild, K. J., & Khorana, H. G. (1991). The reaction of hydroxylamine with bacteriorhodopsin studied with mutants that have altered photocycles: Selective reactivity of different photointermediates. *Proceedings of the National Academy of Sciences of the United States of America*, 88(6), 2583–2587.
  50. Rouso, I., Gat, Y., Lewis, A., Sheves, M., & Ottolenghi, M. (1998). Effective light-induced hydroxylamine reactions occur with C13=C14 nonisomerizable bacteriorhodopsin pigments. *Biophysical Journal*, 75(1), 413–417.
  51. Hasson, K. C., Gai, F., & Anfinrud, P. A. (1996). The photoisomerization of retinal in bacteriorhodopsin: Experimental evidence for a three-state model. *Proceedings of the National Academy of Sciences of the United States of America*, 93(26), 15124–15129.
  52. Hontani, Y., Marazzi, M., Stehfest, K., Mathes, T., Van Stokkum, I. H. M., Elstner, M., et al. (2017). Reaction dynamics of the chimeric channelrhodopsin. *Scientific Reports*, 7(1), 1–12.
  53. Kato, H. E., Zhang, F., Yizhar, O., Ramakrishnan, C., Nishizawa, T., Hirata, K., et al. (2012). Crystal structure of the channelrhodopsin light-gated cation channel. *Nature*, 482(7385), 369–374.
  54. Oesterhelt, D., Hegemann, P., & Tittor, J. (1985). The photocycle of the chloride pump halorhodopsin. II: Quantum yields and a kinetic model. *The EMBO Journal*, 4(9), 2351–2356.
  55. Liang, R., Yu, J. K., Meisner, J., Liu, F., & Martinez, T. J. (2021). Electrostatic control of photoisomerization in channelrhodopsin 2. *Journal of the American Chemical Society*, 143(14), 5425–5437.
  56. Losi, A., Wegener, A. A., Engelhard, M., & Braslavsky, S. E. (2001). Thermodynamics of the early steps in the photocycle of natronobacterium pharaonis halorhodopsin. Influence of medium and of anion substitution†. *Photochemistry and Photobiology*, 74(3), 495.